energies

MDPI

Article

A Study on Performance and Characteristic Analysis According to the Operating Point of IPMSM Drive

Hyun-Jong Park [1], Han-Woong Ahn [2] and Sung-Chul Go [3,*]

[1] Department of Electrical Engineering, Hanyang University, Seoul 04763, Republic of Korea
[2] Satellite Technology Research and Development Division, Korea Aerospace Research Institute, Daejeon 34133, Republic of Korea
[3] Department of Robot Engineering, KEIMYUNG University, Daegu 42601, Republic of Korea
* Correspondence: go@kmu.ac.kr

Abstract: This study presents the characteristics and performance of a motor at the operating point based on pulse-width modulation (PWM). PWM is used in modulating the output voltage of a three-phase inverter. The PWM technique has advantages and disadvantages depending on the system size and operating range. For example, some discontinuous pulse-width modulation (DPWM) techniques are advantageous in low-cost systems because they can reduce the number of switches. Some PWM techniques are complicated for software construction and require a lot of computation. In this paper, PWM techniques were constructed by using the offset voltage injection method. Therefore, the construction of the PWM technique is simplified by the method. In an experimental setup, an interior permanent-magnet synchronous motor (IPMSM) and a three-phase inverter were implemented to test motor control performance depending on the PWM technique. In addition, the current control characteristics and inverter efficiency were analyzed and compared depending on the speed and load of the motor. According to the results of this paper, it is possible to compare the motor and inverter control characteristics using various types of PWM rapidly. Additionally, it will help to select an appropriate PWM technique for a specific system.

Keywords: pulse-width modulation; inverter efficiency; IPMSM driver; offset voltage; CPWM; DPWM

Citation: Park, H.-J.; Ahn, H.-W.; Go, S.-C. A Study on Performance and Characteristic Analysis According to the Operating Point of IPMSM Drive. *Energies* **2023**, *16*, 1219. https://doi.org/10.3390/en16031219

Academic Editor: Gianluca Brando

Received: 11 November 2022
Revised: 14 January 2023
Accepted: 19 January 2023
Published: 22 January 2023

1. Introduction

Several efforts have been made to improve the performance of electric machines in various industrial zones to protect the environment. Particularly, adequate investments have been made in developing higher efficiency electric devices because of social de-mands, such as the reduction in fossil fuel consumption, carbon dioxide emission, and an in-crease in efficiency [1–6]. In the automotive industry, studies on electric and hybrid electric vehicles are underway. Additionally, home electronic appliance industries have invested in developing high-efficiency motors for vacuum cleaners, washing machines, and air conditioners. Electric motors and inverters are key components of these industries.

The inverter generates AC power with a variable frequency and voltage magnitude by switching the power devices. Modulations, such as sinusoidal pulse-width modulation (SPWM) and space-vector pulse-width modulation (SVPWM), are commonly used to generate AC currents [7–11]. Numerous studies have been conducted to fabricate high-performance power devices and microprocessors, to improve the inverter efficiency, reduce the harmonic components of currents, and develop PWM techniques [12–19]. Therefore, various PWM techniques, such as third-harmonic injection pulse-width modulation (THPWM), discontinuous pulse-width modulation (DPWM), and hybrid PWM, have been applied in many applications [20–26].

CPWM (continuous PWM) includes SPWM, SVPWM, and THPWM. SPWM is the most widely used method because it is easy to implement. However, since the voltage command has only the fundamental wave component, it cannot be used in the overmodulation region.

Therefore, compared to other methods, the speed and torque range of the motor control is limited. For SVPWM, since the output voltage of the inverter is converted to a space vector, it has a wide range of output voltage. However, it is difficult to build in software because it requires complicated calculations, such as converting the voltage to a space vector and determining the switching time of each switch. THPWM is a technique of injecting a third harmonic component into the voltage command. Therefore, it is possible to expand the fundamental component to the overmodulation region by reducing the peak value of the voltage command. In other words, it helps to improve motor performance in the region above the rated point, especially at high speeds [27,28].

DPWM is a technique whereby the switching of one phase ceases in a specific region of one cycle, in other words, the phase is clamped to one side of the DC bus. Since the DPWM method reduces the number of switches, the switching loss of the inverter can be minimized. Additionally, it has the advantage of generating a voltage command in the overmodulation area like SVPWM and THPWM. However, reducing the number of switches may increase the harmonic components of the current that cause the torque ripple. In addition, there are various DPWM methods according to the on and off cycles, and their performance is different to the size of the motor and inverter and the speed and load of the motor driving point.

The implementation of some PWM techniques in the motor control algorithm is challenging and requires time to calculate the switching sequences. Therefore, the offset voltage method is a better option for configuring the switching algorithm. This method adds the offset voltage to the reference voltage, and the switching sequence is determined by comparing the reference voltage and the carrier wave. This study presents the offset voltage equation for each PWM technique.

This study analyzed the characteristics of an interior permanent-magnet synchronous motor (IPMSM) at its driving points using various PWM techniques with the offset voltage injection method by simulations and experiments. Additionally, three CPWM and six DPWM techniques with the voltage injecting method are covered, and the simulations and experiments with six techniques are carried out. In particular, test results according to speed and load in the rated operating and field-weakening control are presented, so that the characteristics of the IPMSM and PWM techniques are examined depending on the driving point. Additionally, the torque is analyzed by the current harmonics. This is different from the previous studies that presented the control results for the R-L load, induction motor, or one driving point of the motor [23–26]. The performance characteristics were analyzed through current harmonic analysis and motor torque. Finally, the efficiency of the inverter is experimentally validated.

2. Pulse-Width Modulation Method

2.1. Sinusoidal Pulse-Width Modulation

SPWM is the most commonly used voltage modulation technique to obtain a controlled three-phase output voltage. As shown in Figure 1, the switching states are determined by comparing the triangular carrier wave with the sinusoidal reference voltage. Wherein V_{an}^{*} is the phase A to ground voltage. The maximum modulation index (MI) is 1. The MI is the ratio of the fundamental component of the inverter output voltage to half of the DC bus voltage. The reference pole voltage is a sinusoidal waveform with the desired magnitude and frequency and can be designed using an analog circuit. Therefore, SPWM is commonly used in various industrial applications, and because the sampling time is controlled, it exhibits excellent dynamic characteristics.

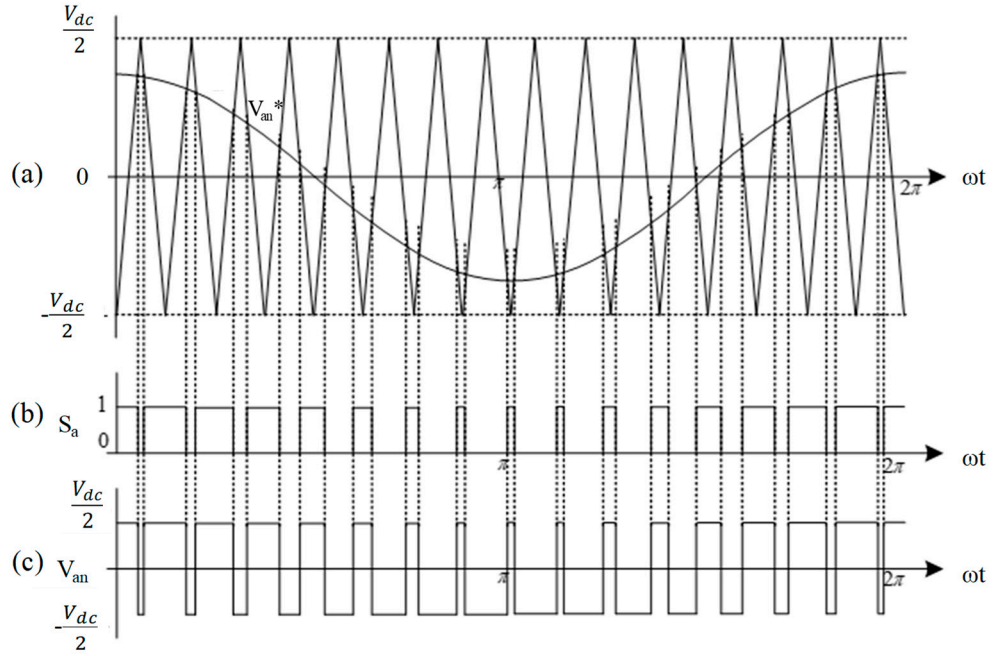

Figure 1. SPWM technique for phase a of a motor (**a**) reference phase voltage and triangular carrier wave; (**b**) switching state; (**c**) output voltage of the inverter.

2.2. Third-Harmonic Pulse-Width Modulation

THPWM is a voltage modulation method that injects the third-harmonic component into the sinusoidal reference pole voltage, as shown in Equation (1).

$$V_{an}^{*} = A_1 cos(\omega_e t) + A_1 B_1 cos(3\omega_e t) \quad (1)$$

where A_1 is the magnitude of the fundamental component and ω_e is the electrical frequency. Since the third harmonic reduces the peak value of the voltage command, the fundamental component can increase to larger than 1. Generally, B_1, which represents the magnitude of the third harmonic, is set to $-1/6$ and it may be increased MI to 1.155. In the THPWM technique, the peak value of the phase voltage is smaller than the pole voltage; thus, the maximum MI is $2/\sqrt{3}$. However, because of the injected third-harmonic component, it has the disadvantage of poor current control performance.

2.3. Space Vector Pulse-Width Modulation

The SVPWM is a popular motor control technique. It has fewer harmonic components in the output current and torque than other PWM techniques; therefore, it is most commonly used for motor control.

As shown in Figure 2, the reference voltage and switching states are represented in the d-q plane. The switching states in a three-phase inverter have eight vectors, and during the control period T_s, the fundamental volt-second average of the reference voltage, V^*, is generated by synthesizing the eight switching states. That is, two voltage vectors (V_n, V_{n+1}) closest to the reference voltage and zero vectors are used to generate the same fundamental voltage as the reference voltage, V^*. The control period of this voltage modulation, T_s, is half that of the switching period.

The range of the fundamental voltage vector with SVPWM is inside the hexagon area. Therefore, the maximum value of the fundamental component of the phase voltage is ap-proximately 15.5% greater than that of the SPWM. Additionally, the SVPWM technique allows an MI of $2/\sqrt{3}$.

In the SVPWM technique, calculating the sequence and switching time of switching states is complex and requires more time than in other PWM techniques. However, these problems can be solved using the offset voltage injection method discussed in Section 3.

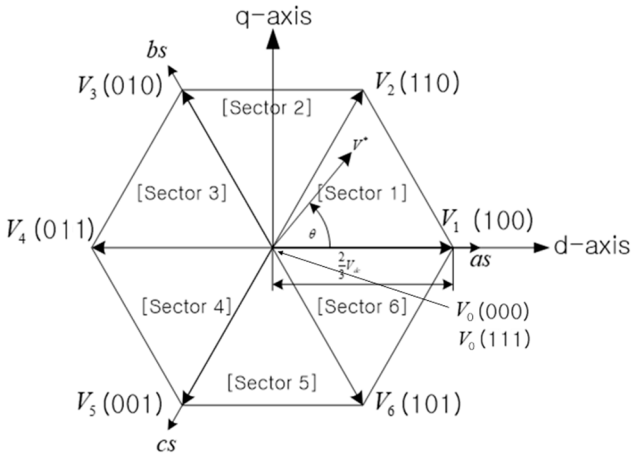

Figure 2. Switching states of the SVPWM technique.

2.4. Discontinuous Pulse-Width Modulation

The DPWM technique is used to decrease the number of switching sequences. The switching loss of the inverter is decreased using the DPWM technique. To reduce the switching loss, the switches in the phase with the largest current value are generally kept off. However, in the case of DPWM, since switch states are not changed for 1/3 cycles, the effective switching frequency is reduced by 2/3 times.

The 60° DPWM technique is the most common one. In Figure 3a, the switching state of phase A is 1 in the 60° range, where the reference voltage of phase A is larger than that of the others. Additionally, it is zero in the 60° range when the reference voltage of phase A is low. The output voltage of the inverter is $V_{dc}/2$ when the switching state of phase A is 1 and $-V_{dc}/2$ when the switching state is zero. In the 60° DPWM technique, the usage of switches decreases by 1/3 compared with CPWM.

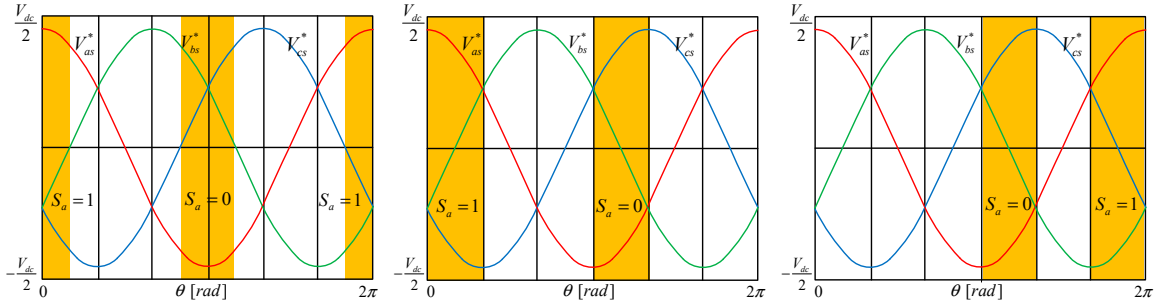

Figure 3. The 60° discontinuous PWM technique: (**a**) 60° DPWM; (**b**) 60° (+30°) DPWM; (**c**) 60° (−30°) DPWM.

To optimize the reduction in switching loss, the switching state should be determined preferably using the phase current, not the voltage. Therefore, the switching states in DPWM consider the power factor. If the system has a lagging power factor, then selecting the 60° (+30°) DPWM technique in Figure 3b is preferable. However, if the system has a leading power factor, the 60° (−30°) DPWM technique in Figure 3b is preferable.

The 30° DPWM technique, shown in Figure 4a, is remarkable in reducing harmonic component losses as another DPWM. Additionally, the 120° DPWM in Figure 4b,c is for a lower cost system. It includes 120° (on) and 120° (off) DPWM. This technique is ineffective in reducing harmonics but can reduce the number of switching operations.

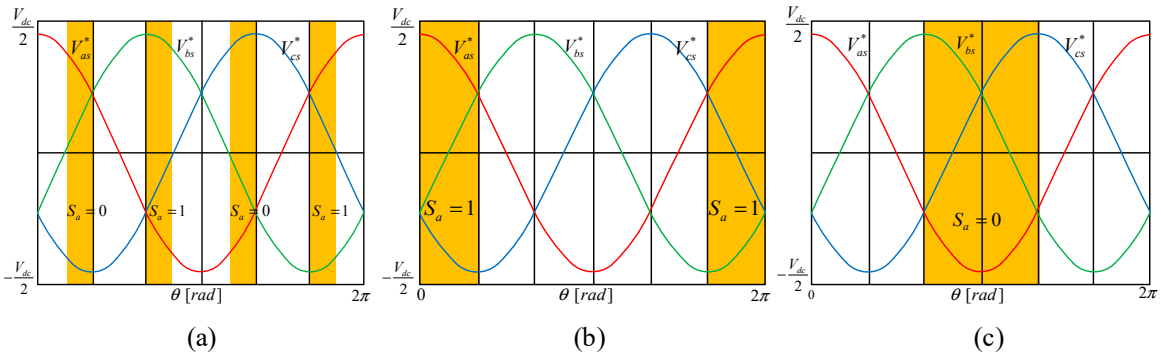

Figure 4. Discontinuous PWM technique: (**a**) 30° DPWM; (**b**) 120° (on) DPWM; (**c**) 120° (off) DPWM.

The switching loss of the inverter is reduced with DPWMs; nevertheless, the harmonic components in the phase currents increase when MI is low. However, it performs better than CPWM when the MI is higher.

3. The Offset Voltage Injection Method

The entire speed control block for the IPMSM is shown in Figure 5a, wherein the PI controllers are constructed for the speed and current control. It is composed based on vector control, and the subscripts d and q mean the physical quantities on the d-axis and q-axis, respectively. Figure 5b shows a magnified view of the red block in Figure 5a, which shows the PWM with the offset voltage injection method. Wherein v_{an} is the phase A to ground voltage, v_{as} is the phase A to neutral voltage, and v_{sn} is the offset voltage. Some PWM techniques are complicated for software construction, and the offset voltage injection method simplifies it. This section introduces the offset voltage equations for each PWM.

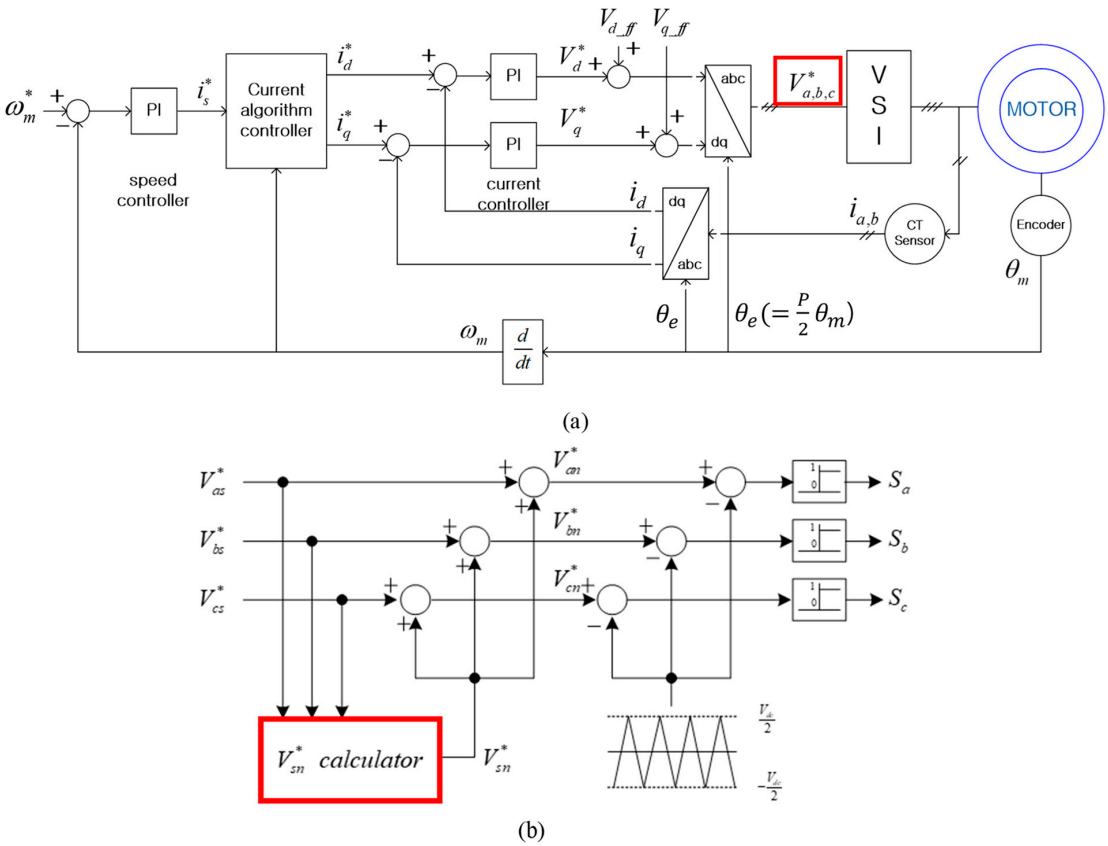

Figure 5. Control block for IPMSM speed control: (**a**) IPMSM control algorithm; (**b**) switching function for injecting the offset voltage.

3.1. SPWM and THPWM

In the SPWM technique, the reference pole and reference phase voltages are identical. Therefore, the offset voltage (V_{sn}) is zero.

In the THPWM technique, a third-harmonic component with a fundamental phase voltage of $-1/6$ is injected into the reference voltage. Therefore, the offset voltage is the same as that of the third-harmonic component. The reference voltage is given by (2), and its third-harmonic component is expressed in (3),

$$V_{as}^{*} = V_m cos\theta, \tag{2}$$

$$V_{sn} = -\frac{V_m}{6} cos(3\theta) = -\frac{V_m}{6}\left(4\left(\frac{V_{as}^{*}}{V_m}\right)^3 - 3\frac{V_{as}^{*}}{V_m}\right). \tag{3}$$

Using the magnitude of the reference phase voltages and Kirchhoff's rule, Equations (4) and (5) are given as

$$V_m = \sqrt{\frac{2}{3}\left(V_{as}^{*2} + V_{bs}^{*2} + V_{cs}^{*2}\right)}, \tag{4}$$

$$V_{as}^{*} + V_{bs}^{*} + V_{cs}^{*} = 0. \tag{5}$$

The offset voltage for THPWM in Equation (6) is written using Equations (3)–(5) as

$$V_{sn} = -\frac{V_{as}^{*} V_{bs}^{*} V_{cs}^{*}}{V_{as}^{*2} + V_{bs}^{*2} + V_{cs}^{*2}}, \tag{6}$$

3.2. Space Vector Pulse-Width Modulation

As shown in Figure 6, the concept of calculating the offset voltage for SVPWM arranges the effective voltage to the center of one modulation cycle.

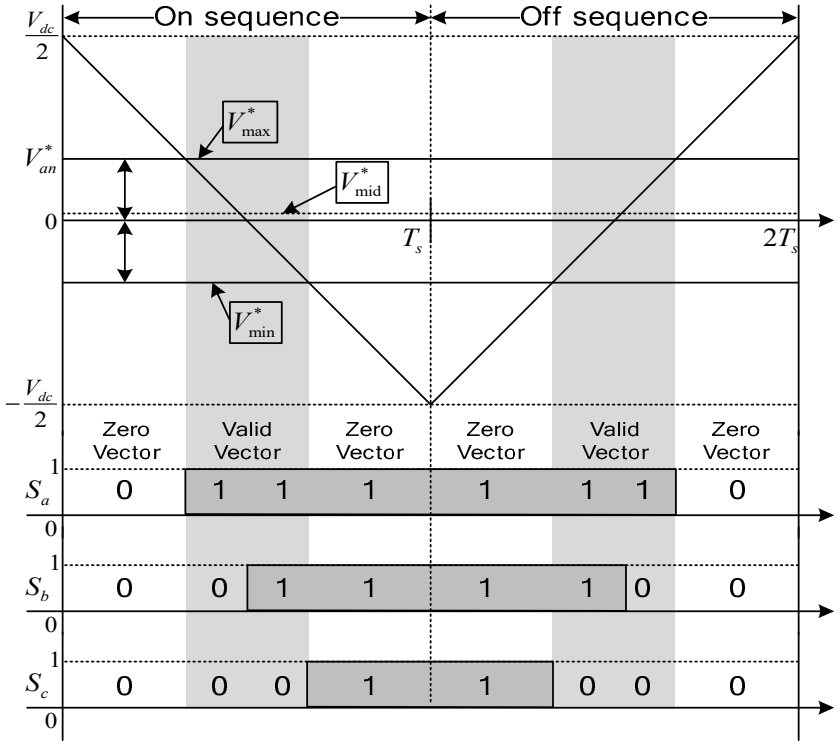

Figure 6. Technique for symmetric SVPWM.

Therefore, the offset voltage of the SVPWM is written as Equations (7) and (8), setting the absolute values of the maximum and minimum pole voltages to be the same.

$$V^*_{max} + V_{sn} = -(V^*_{min} + V_{sn}), \tag{7}$$

$$V_{sn} = -\frac{V^*_{max} + V^*_{min}}{2}. \tag{8}$$

Figure 7 shows the relationships between the reference voltages of CPWMs from simulations, wherein the reference pole voltage (V_{an}) was obtained by injecting the offset voltage (V_{sn}) into the sinusoidal reference phase voltage (V_{as}). Figure 7a–c represent the voltage relations of SPWM, THPWM, and SVPWM, respectively.

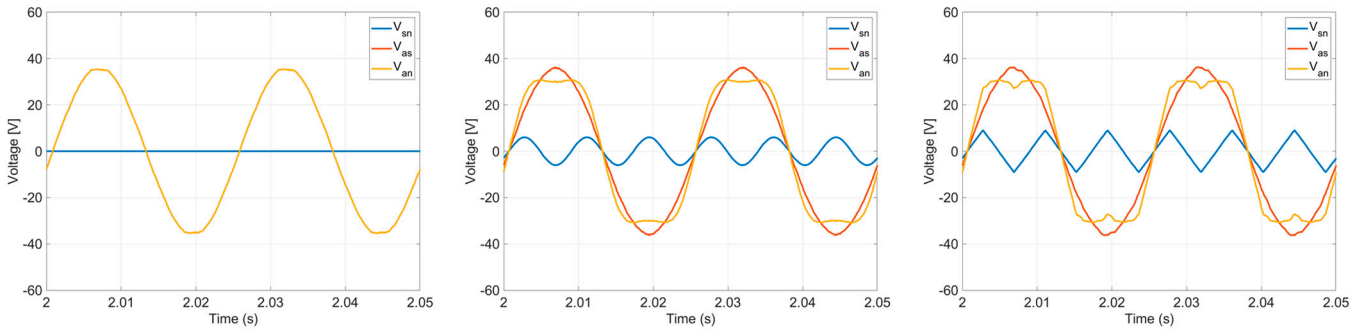

(a) (b) (c)

Figure 7. Voltage relationships of the CPWM: (**a**) SPWM; (**b**) THPWM; (**c**) SVPWM.

3.3. Sixty-Degrees Discontinuous Pulse-Width Modulation

As shown in Figure 3b, for the 60° DPWM technique, the switching state is one or zero in the 60° range when the reference voltage of one phase is the maximum or mini-mum, respectively. Accordingly, the offset voltage of the 60° DPWM is expressed as follows:

$$\begin{aligned} V_{sn} &= \tfrac{V_{dc}}{2} - V^*_{max} \ (when\ V^*_{max} + V^*_{min} \geq 0) \\ V_{sn} &= -\tfrac{V_{dc}}{2} - V^*_{min} \ (when\ V^*_{max} + V^*_{min} < 0). \end{aligned} \tag{9}$$

The reference pole voltage (V_{an}) was obtained by injecting the offset voltage (V_{sn}) into the reference phase voltage (V_{as}), as shown in Figure 8.

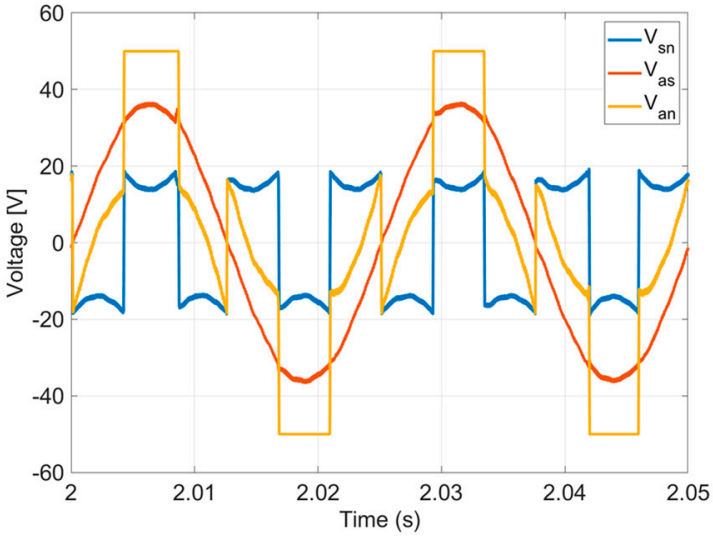

Figure 8. Voltage relations of 60° DPWM.

The 60° (+30°) DPWM and 60° (−30°) DPWM techniques are shown in Figure 3b,c, respectively. The voltage equations of the 60° (+30°) DPWM can be expressed as follows:

$$\begin{aligned} V_{sn} &= \tfrac{V_{dc}}{2} - V_{cs}^{*}\ (when\ V_{as}^{*} = V_{\text{mid}}^{*}\ and\ V_{cs}^{*} \geq 0), \\ V_{sn} &= -\tfrac{V_{dc}}{2} - V_{cs}^{*}\ (when\ V_{as}^{*} = V_{\text{mid}}^{*}\ and\ V_{cs}^{*} < 0), \\ V_{sn} &= \tfrac{V_{dc}}{2} - V_{as}^{*}\ (when\ V_{bs}^{*} = V_{\text{mid}}^{*}\ and\ V_{as}^{*} \geq 0), \\ V_{sn} &= -\tfrac{V_{dc}}{2} - V_{as}^{*}\ (when\ V_{bs}^{*} = V_{\text{mid}}^{*}\ and\ V_{as}^{*} < 0), \\ V_{sn} &= \tfrac{V_{dc}}{2} - V_{bs}^{*}\ (when\ V_{cs}^{*} = V_{\text{mid}}^{*}\ and\ V_{bs}^{*} \geq 0), \\ V_{sn} &= -\tfrac{V_{dc}}{2} - V_{bs}^{*}\ (when\ V_{cs}^{*} = V_{\text{mid}}^{*}\ and\ V_{bs}^{*} < 0). \end{aligned} \tag{10}$$

Moreover, the voltage equations of the 60° (−30°) DPWM can be expressed as follows:

$$\begin{aligned} V_{sn} &= \tfrac{V_{dc}}{2} - V_{bs}^{*}\ (when\ V_{as}^{*} = V_{\text{mid}}^{*}\ and\ V_{bs}^{*} \geq 0), \\ V_{sn} &= -\tfrac{V_{dc}}{2} - V_{bs}^{*}\ (when\ V_{as}^{*} = V_{\text{mid}}^{*}\ and\ V_{bs}^{*} < 0), \\ V_{sn} &= \tfrac{V_{dc}}{2} - V_{cs}^{*}\ (when\ V_{bs}^{*} = V_{\text{mid}}^{*}\ and\ V_{cs}^{*} \geq 0), \\ V_{sn} &= -\tfrac{V_{dc}}{2} - V_{cs}^{*}\ (when\ V_{bs}^{*} = V_{\text{mid}}^{*}\ and\ V_{cs}^{*} < 0), \\ V_{sn} &= \tfrac{V_{dc}}{2} - V_{as}^{*}\ (when\ V_{cs}^{*} = V_{\text{mid}}^{*}\ and\ V_{as}^{*} \geq 0), \\ V_{sn} &= -\tfrac{V_{dc}}{2} - V_{as}^{*}\ (when\ V_{cs}^{*} = V_{\text{mid}}^{*}\ and\ V_{as}^{*} < 0). \end{aligned} \tag{11}$$

The relationships between the reference voltages of the 60° (+30°) DPWM and the 60° (−30°) DPWM are shown in Figure 9a,b.

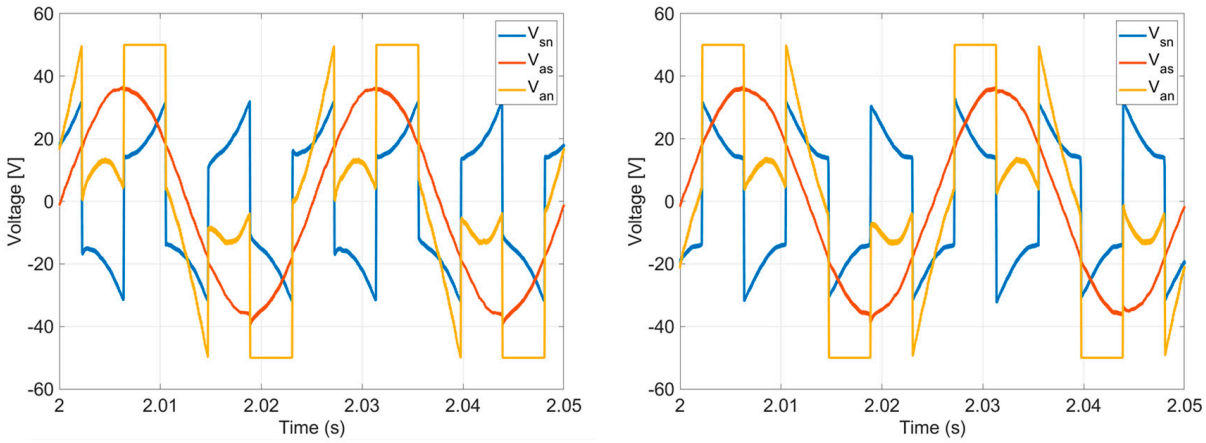

Figure 9. Voltage relationships of the 60° DPWM: (**a**) 60° (+30°) DPWM;(**b**) 60° (−30°) DPWM.

3.4. Other Discontinuous Pulse-Width Modulations

The 30° DPWM in Figure 4a has a complementary relationship with the 60° DPWM. Therefore, the offset voltage can be written as follows:

$$\begin{aligned} V_{sn} &= -\tfrac{V_{dc}}{2} - V_{min}^{*}\ (when\ V_{max}^{*} + V_{min}^{*} \geq 0) \\ V_{sn} &= \tfrac{V_{dc}}{2} - V_{max}^{*}\ (when\ V_{max}^{*} + V_{min}^{*} < 0). \end{aligned} \tag{12}$$

The 120° (on) DPWM and the 120° (off) DPWM in Figure 4b,c can be expressed as Equations (13) and (14), respectively:

$$V_{sn} = \frac{V_{dc}}{2} - V_{max}^{*}, \tag{13}$$

$$V_{sn} = -\frac{V_{dc}}{2} - V^*_{min}. \quad (14)$$

The reference voltage relationships between these are shown in Figure 10.

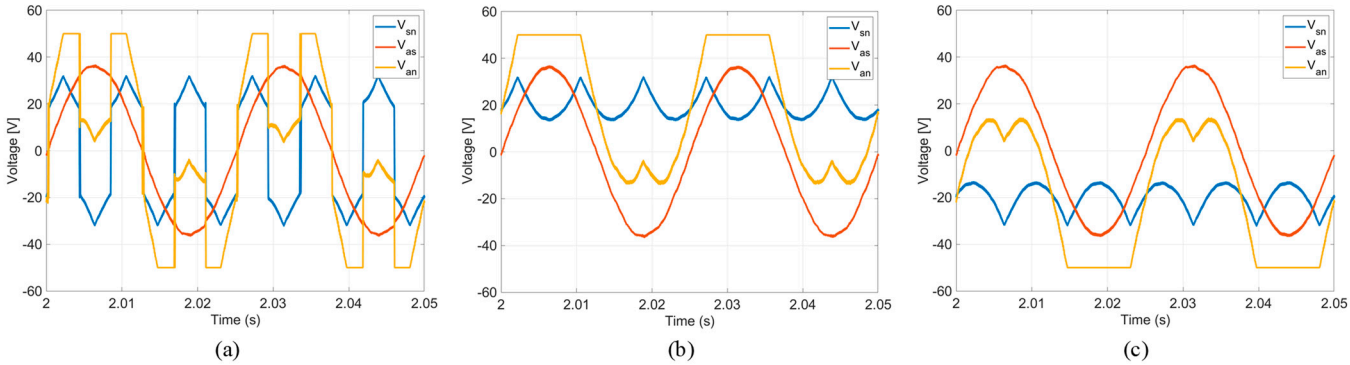

Figure 10. Voltage relations of other DPWMs: (**a**) +30° DPWM; (**b**) 120° (on) DPWM; (**c**) 120° (off) DPWM.

4. Test Results of the IPMSM

4.1. Simulation Results

The specifications of the IPMSM for the simulation are listed in Table 1. The simulation was conducted by configuring the block diagram shown in Figure 5. In the simulation, the back EMF of the IPMSM was assumed to be a sinusoidal wave, and the cogging torque was set to be 0. At this time, 10 kHz switching frequency was applied to all PWMs in simulations and experiments. The test simulated driving the motor at the desired speed through speed control with applying load torque to the motor. Conversely, in the experiment in the following section, current control was performed when the motor was driving at a constant speed, as measured by the dynamometer. The following figures show the simulation results when the IPMSM was controlled at 400 rpm and 1.6 Nm of load torque and 1500 rpm and 1.0 Nm.

Table 1. IPMSM specifications.

Variables	Value	Unit
Resistance	2.85	Ohm
Rated speed	1250	rpm
DC Supply Voltage	100	V
Rated current	3.25	A
Number of Poles	8	-
d-axis inductance	20.26	mH
q-axis inductance	22.67	mH

The simulation results in Figures 11 and 12 show the current harmonics and motor torque in the steady state section when the desired speed is 400 rpm with 1.6 Nm of load torque. In the case of the harmonic components in Figure 11, the harmonics of 120 DPWM are relatively high except for the third- and sixth-order harmonics, but the harmonics of SPWM and 60° DPWM are relatively small. Additionally, the fifth- and seventh-order harmonics of SVPWM are higher than other PWMs. The result of the 30° DPM is similar to that of the 120° DPWM. Figure 12a–f show the results of SPWM, SVPWM, THPWM, 60° DPWM, 30° DPWM, and 120° (off) DPWM, respectively. In Figure 12, the torque ripple of SPWM and THPWM are slightly smaller, and that of SVPWM and 120° (off) DPWM are similar. This can be understood from the results of the current harmonics that the torque ripple of the sixth-order harmonic is small in SPWM and THPWM where the fifth- and seventh-order current harmonics are small [29]. Additionally, in Figure 12, in the case of the 60° DPWM and the 30° DPWM, the notches are generated in the torque. This occurs in

the switching transition timing when the voltage of Vdc/2 or −Vdc/2 is suddenly applied, and it is the characteristic of DPWM.

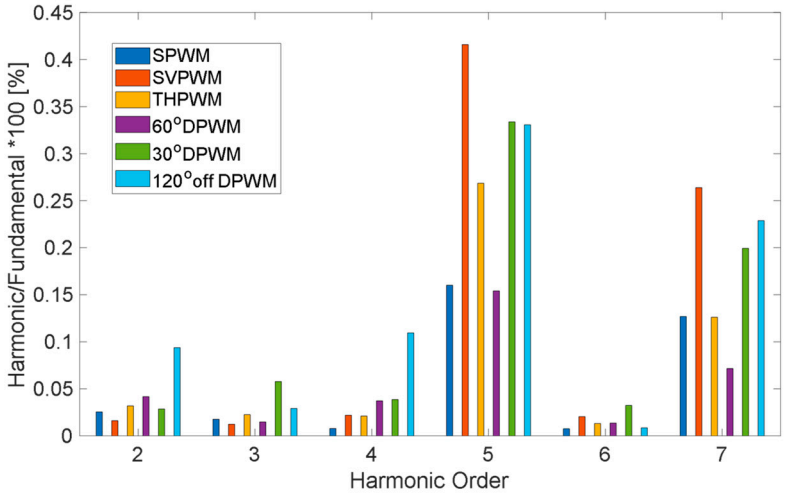

Figure 11. Simulation results of phase current harmonics in steady state at 400 rpm and 1.6 Nm.

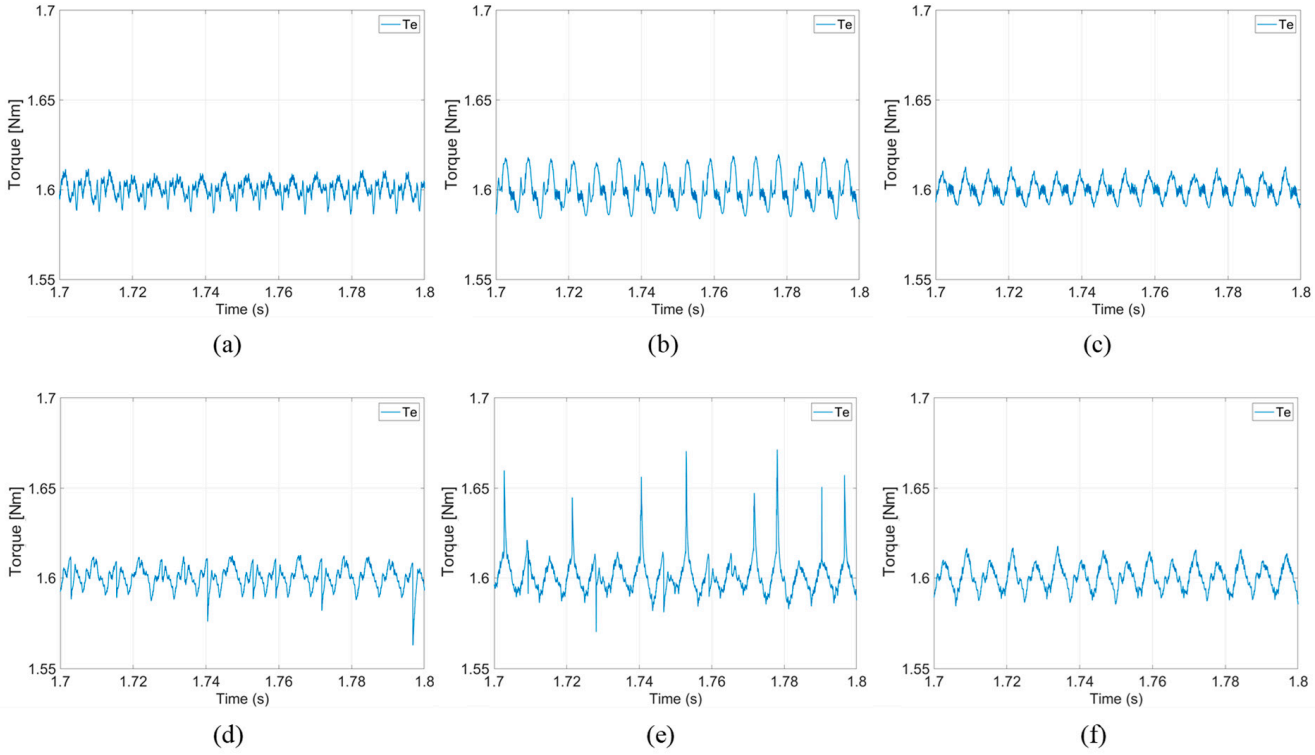

Figure 12. Simulation results of motor torque in steady state at 400 rpm and 1.6 Nm of load torque: (**a**) SPWM; (**b**) THPWM; (**c**) SVPWM; (**d**) 60° DPWM; (**e**) 30° DPWM; (**f**) 120° (off) DPWM.

The simulation results in Figures 13 and 14 show the current harmonics and motor torque when the desired speed is 1500 rpm with 1.0 Nm of load torque. The second- and fourth-order harmonics of 120 DPWM are high and the fifth- and seventh-order harmonics of SPWM are higher than other PWMs. From the following figure, it is confirmed that the fifth and seventh harmonics have a greater effect on the torque ripple than the second and fourth harmonics. Figure 14a–f show the results of SPWM, SVPWM, THPWM, 60° DPWM, 30° DPWM, and 120° DPWM, respectively. Additionally, in Figure 14, the small box at the bottom magnifies the torque for about 0.2 s in the maximum torque section, and the small box at the top shows the torque for about 0.2 s in steady state. The rated speed of this

motor is 1250 rpm, so maximum torque control was performed from 0 to 1250 rpm, and field-weakening control was performed after 1250 rpm. Therefore, in Figure 14, it can be seen that the maximum torque is performed until about 0.35 s, and field-weakening control is performed in the subsequent section. In the maximum torque section, the torque ripple in Figure 14c,d is higher. In Figure 14a, in the case of SPMW, the field-weakening control start time is faster than other PWMs but the settling time is 20% slower. In the field-weakening control section, the torque ripple of SPWM has increased noticeably compared to other results. This shows that the motor control performance rapidly decreases after the rated speed because the MI of SPWM is lower than that of the others. What is noteworthy is that in the case of the 120° DPWM, there is no significant difference in performance compared to SVPWM and THPWM in torque ripple, and the torque ripples of the three methods are similar.

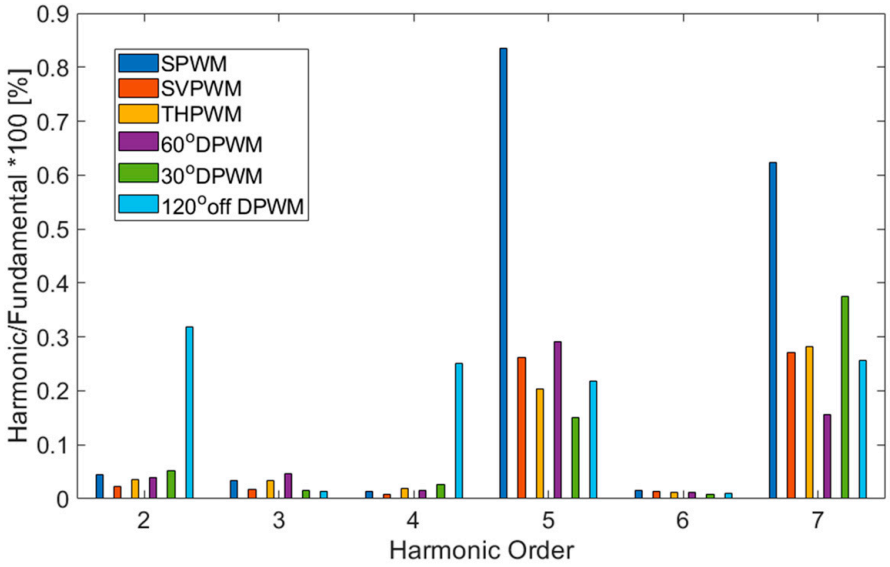

Figure 13. Simulation results of phase current harmonics in steady state at 1500 rpm and 1.0 Nm.

4.2. Experimental Results

An experiment was performed to compare the characteristics of various PWMs. The 5000 W interior permanent-magnet synchronous motor (IPMSM) and experimental setup for the test are shown in Figure 15a,b, respectively. A power analyzer was implemented to measure the efficiency, power factor, and output of the inverter, and an oscilloscope was set to measure the phase voltage and currents of the IPMSM. In the experiment, current control was performed when the motor was driving at a constant speed, as measured by the dynamometer. Additionally, the IPMSM was controlled at speeds of 200 to 1200 rpm, and the load torque varied by the current command at these speeds. Additionally, the current command is same with the peak value of the phase current.

The measured data of phase A from the IPMSM control at 400 and 1000 rpm using SPWM, THPWM, SVPWM, 60° DPWM, 30° DPWM, and 120° (off) DPWM are shown in Figures 16a–f and 17a–f, respectively. The blue, red, and green lines represent the reference phase voltage, reference pole voltage, and phase current, respectively. In these figures, the characteristics of the reference voltages and the phase currents are verified. In particular, the reference pole voltage in the experiment and the simulation results in the previous chapter appeared to be similar, which proves that the speed control using each PWM performs well. Additionally, comparing Figures 16 and 17, it can be confirmed that the sinusoidal current is controlled well at a higher speed since the harmonic component decreased. This is also shown in the next Figures 18 and 19 which shows the harmonics of current and MI values.

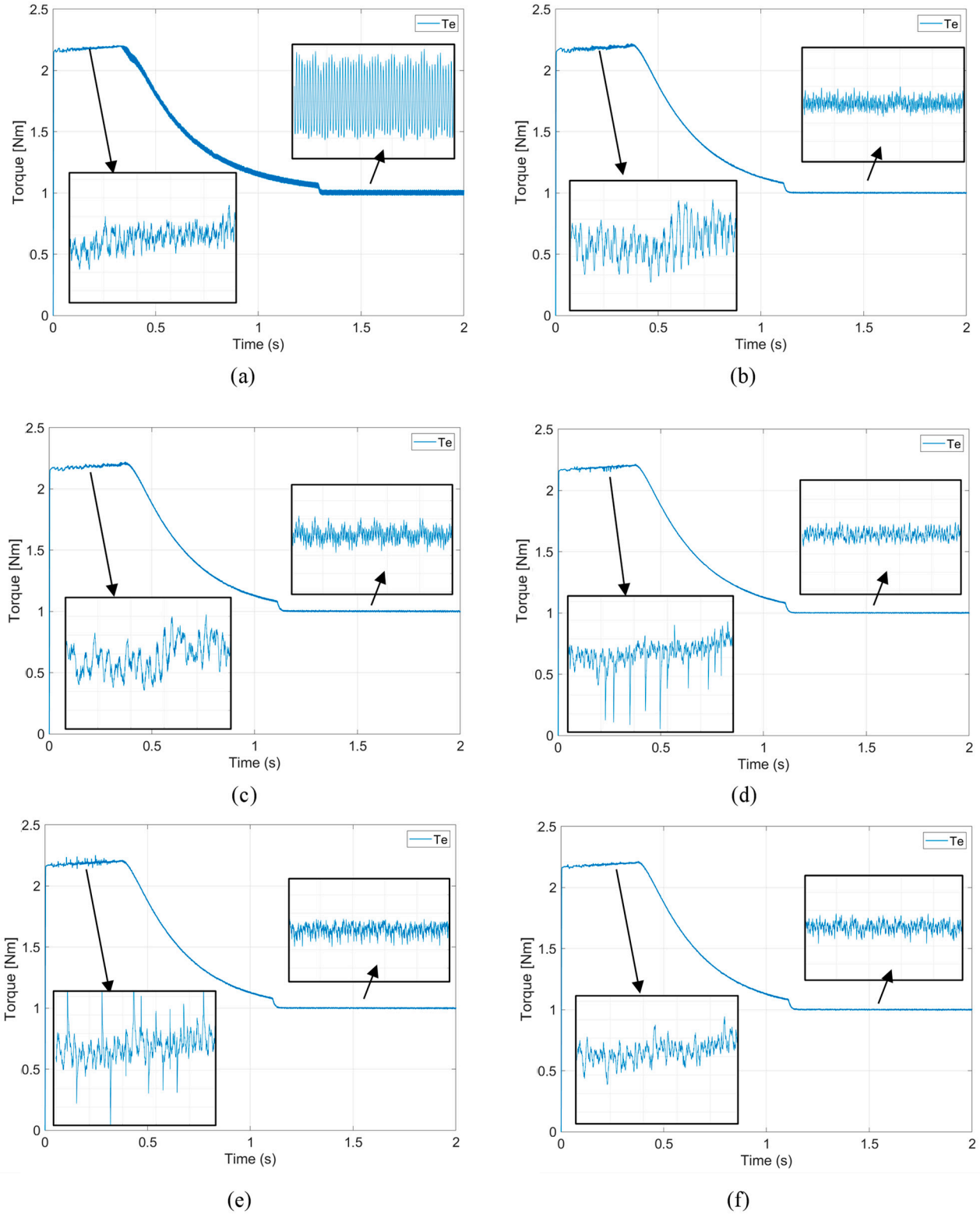

Figure 14. Simulation results of motor torque at 1500 rpm of command and 1.0 Nm of load torque: (**a**) SPWM; (**b**) THPWM; (**c**) SVPWM; (**d**) 60° DPWM; (**e**) 30° DPWM; (**f**) 120° (off) DPWM.

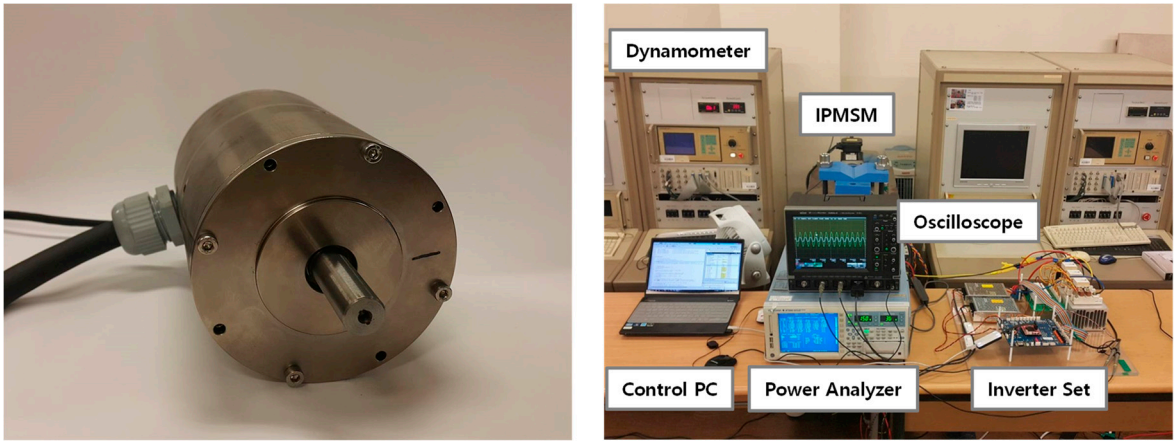

Figure 15. Experimental setup for IPMSM control: (**a**) IPMSM for the experiments; (**b**) experimental setup.

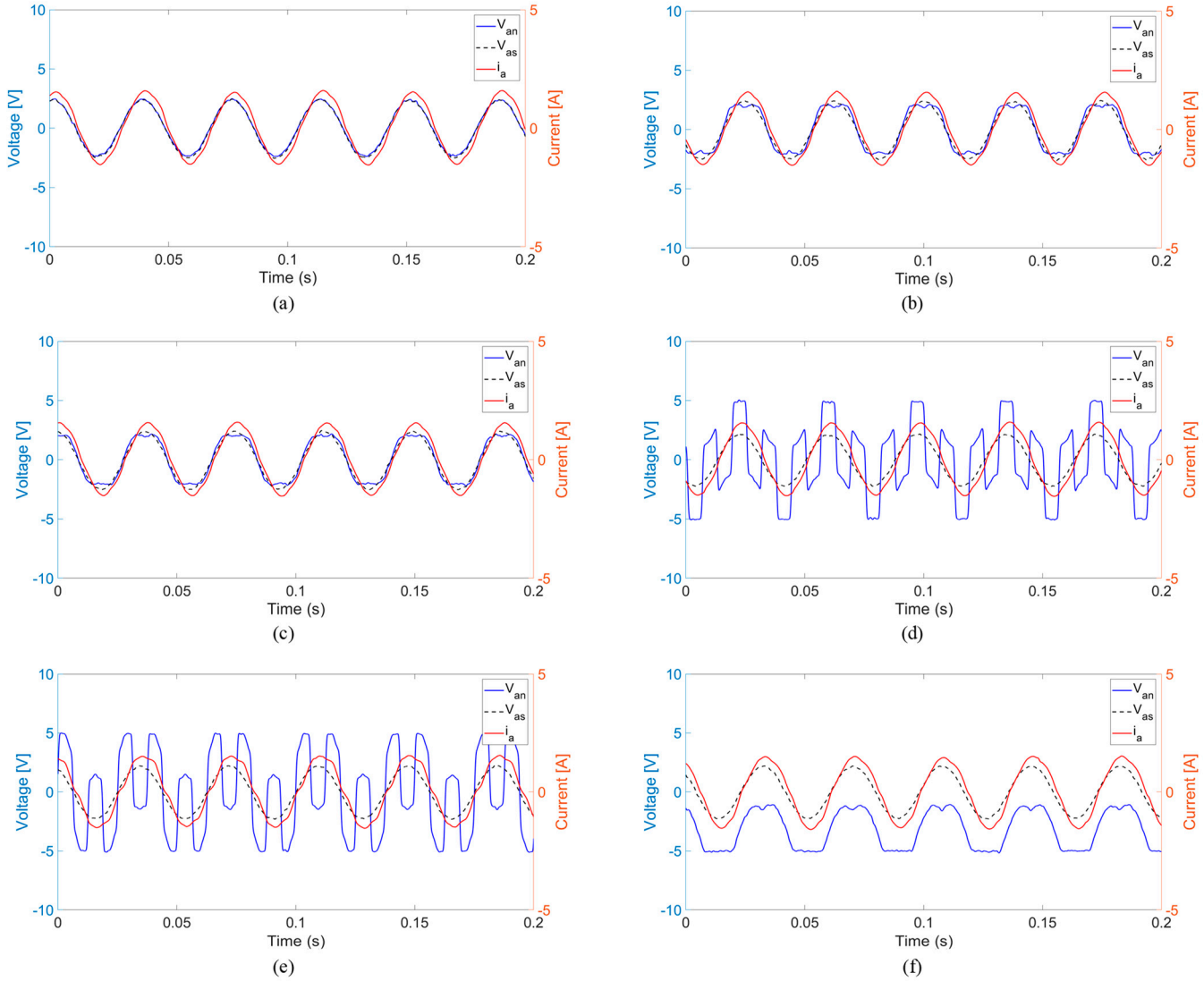

Figure 16. Experimental results at 400 rpm and 1.5 A depending on the PWM technique: (**a**) SPWM; (**b**) THPWM; (**c**) SVPWM; (**d**) 60° DPWM; (**e**) 30° DPWM; (**f**) 120° (off) DPWM.

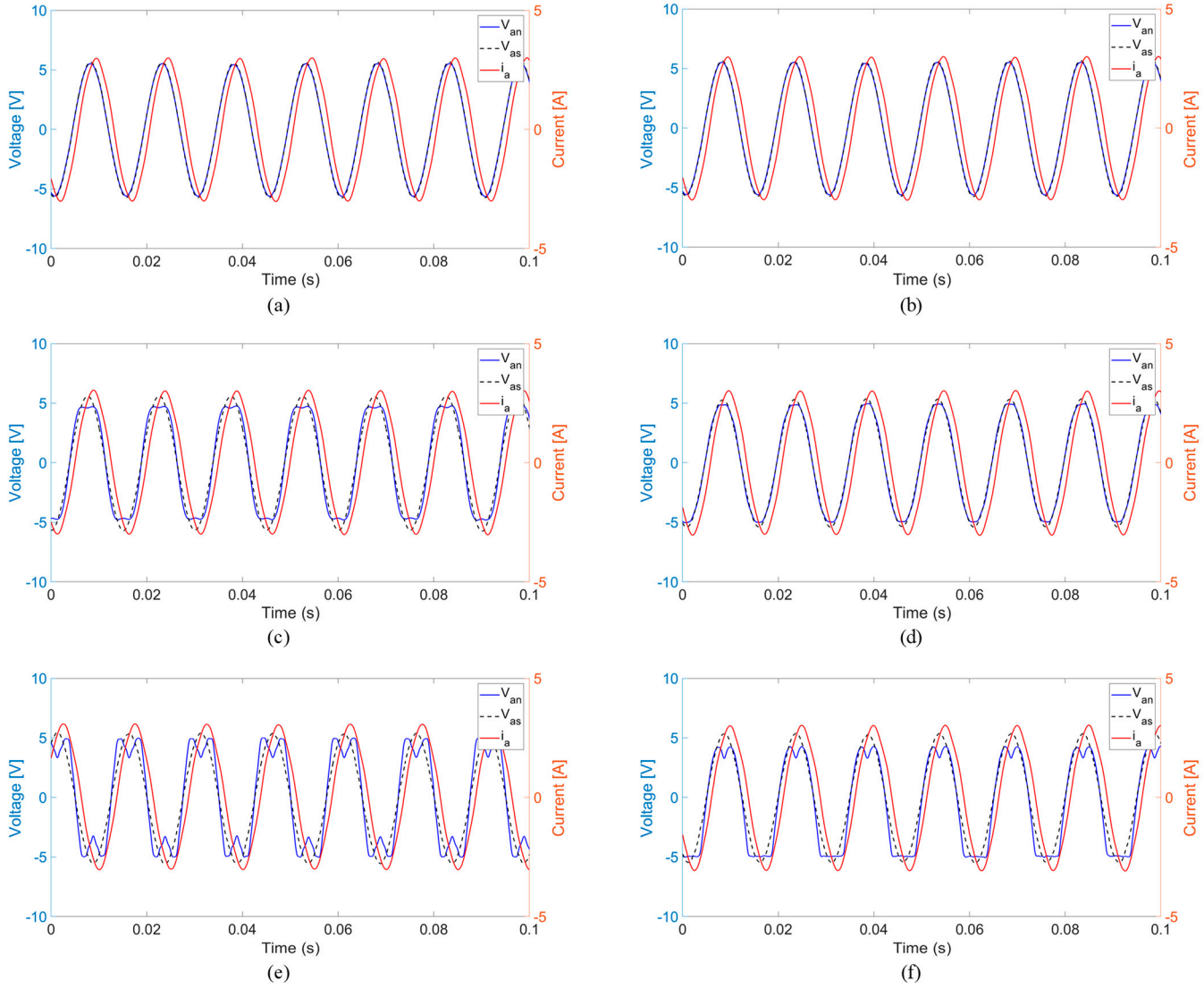

Figure 17. Experimental results at 1000 rpm and 3 A depending on the PWM technique: (**a**) SPWM; (**b**) THPWM; (**c**) SVPWM; (**d**) 60° DPWM; (e) 30° DPWM; (**f**) 120° (off) DPWM.

From the simulation results, the harmonics of the current help to expect the torque ripple. In particular, the fifth and seventh harmonics have a greater effect on the torque ripple. Figure 18 shows the spectrum analysis result for the current waveform in Figures 16 and 17. Figure 18a,b are the results of fundamental and harmonic analysis for phase current at 400 rpm and 1.5 A of current command, respectively, Figure 18c,d show the results at 1000 rpm and 3 A of current command, and Figure 18e,f show the results at 1200 rpm and 3 A of current command. The y-axis represents the ratio of each harmonic to the command magnitude. In Figure 18a, the fundamental components are different by less than 0.5% regardless of the PWM methods. In Figure 18b, the second harmonic in 120° (off) DPWM is three times larger than that of other methods and the second harmonic in SPWM is the smallest. These are similar to the simulation results. Additionally, the fifth and seventh harmonics in the 30° DPWM are twice that of other methods. In Figure 18c, the fundamental components in the 30° PWM and the 120° (off) DPWM are 1% larger than others. In Figure 18d, the overall harmonic components are smaller than the results of 400 rpm in Figure 18b. In Figure 18e, the fundamental components in SPWM are 84% (about 2.5 A) and much smaller than the others. It is confirmed that the current value using SPWM drops sharply as the rated speed is exceeded. In Figure 18f, harmonic components are similar to the trend in Figure 18d.

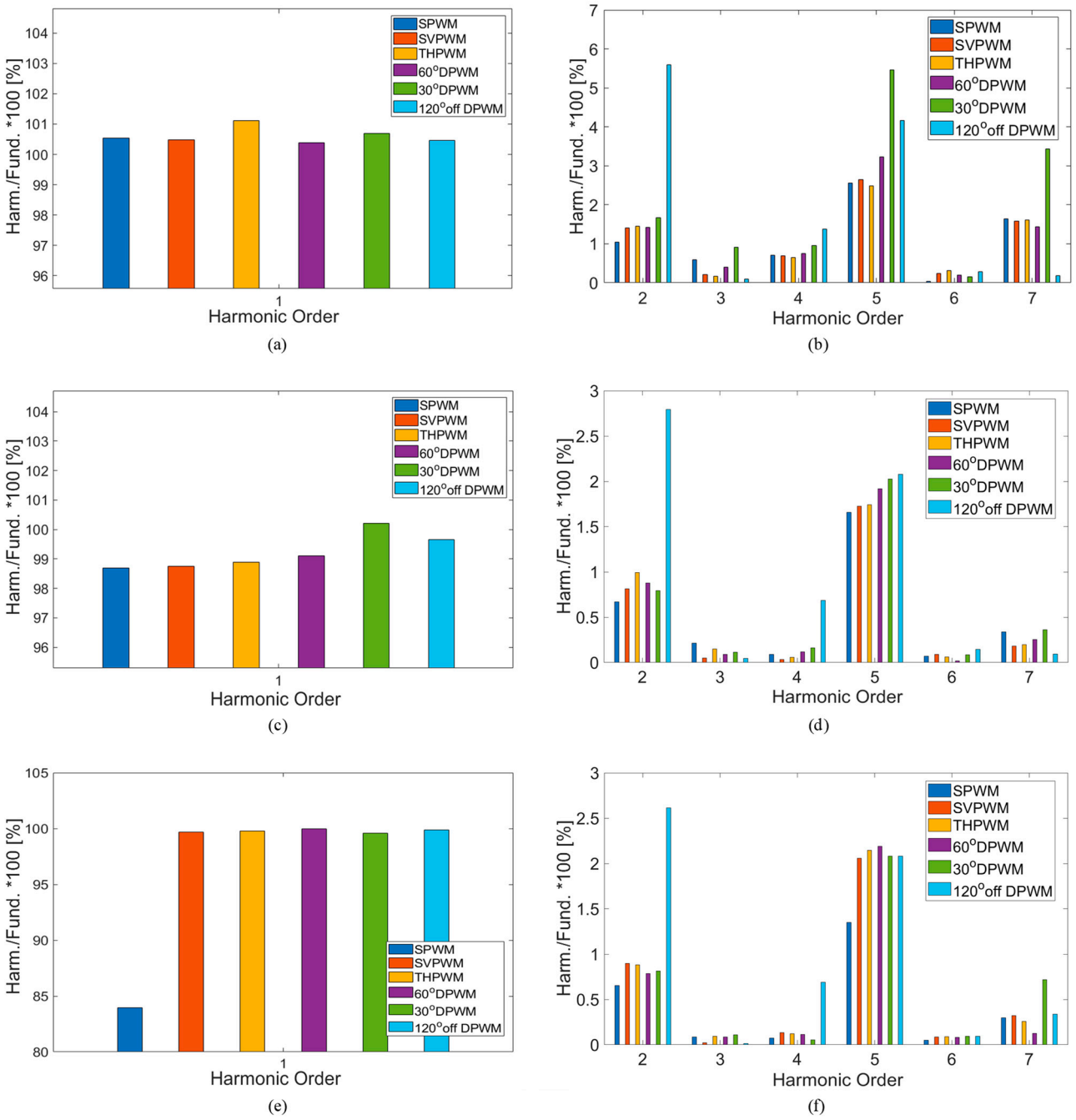

Figure 18. Spectrum of phase current depending on the PWM technique: (**a**) fundamental component at 400 rpm and 1.5 A; (**b**) harmonics at 400 rpm and 1.5 A; (**c**) fundamental component at 1000 rpm and 3 A; (**d**) harmonics at 1000 rpm and 3 A; (**e**) fundamental component at 1200 rpm and 3 A; (**f**) harmonics at 1200 rpm and 3 A.

The torque per voltage MI (TPV) depending on the PWM technique is shown in Figure 19. The value means the unit voltage required to generate torque. In other words, if the TPV is large, it requires less voltage to generate the same torque. Overall, the TPV of the DPWM techniques is higher than those of the CPWM techniques. In fact, in the experiment of the same current command, the MI of DPWM was measured to be relatively low. It seems that the effective voltage of DPWM is high at the same current command because the number of switches is small, and the dead time is reduced accordingly. Therefore, CPWM techniques have a more fundamental component of phase voltage to generate the desired current. It is also shown in Figure 18 that CPWM has relatively fewer harmonics than

DPWM from the current spectrum data. Additionally, in general, at low MI, the voltage harmonics of DPWM are larger than those of CPWM, and the effective switching frequency of DPWM is small, so the harmonics relatively increase [30]. In Figure 19d, the results of SPWM at 1200 rpm are decreased by increasing the current command, since the MI of SPWM is 85%, theoretically. It is confirmed that the performance of the current control with SPWM is not completely over the rated driving point.

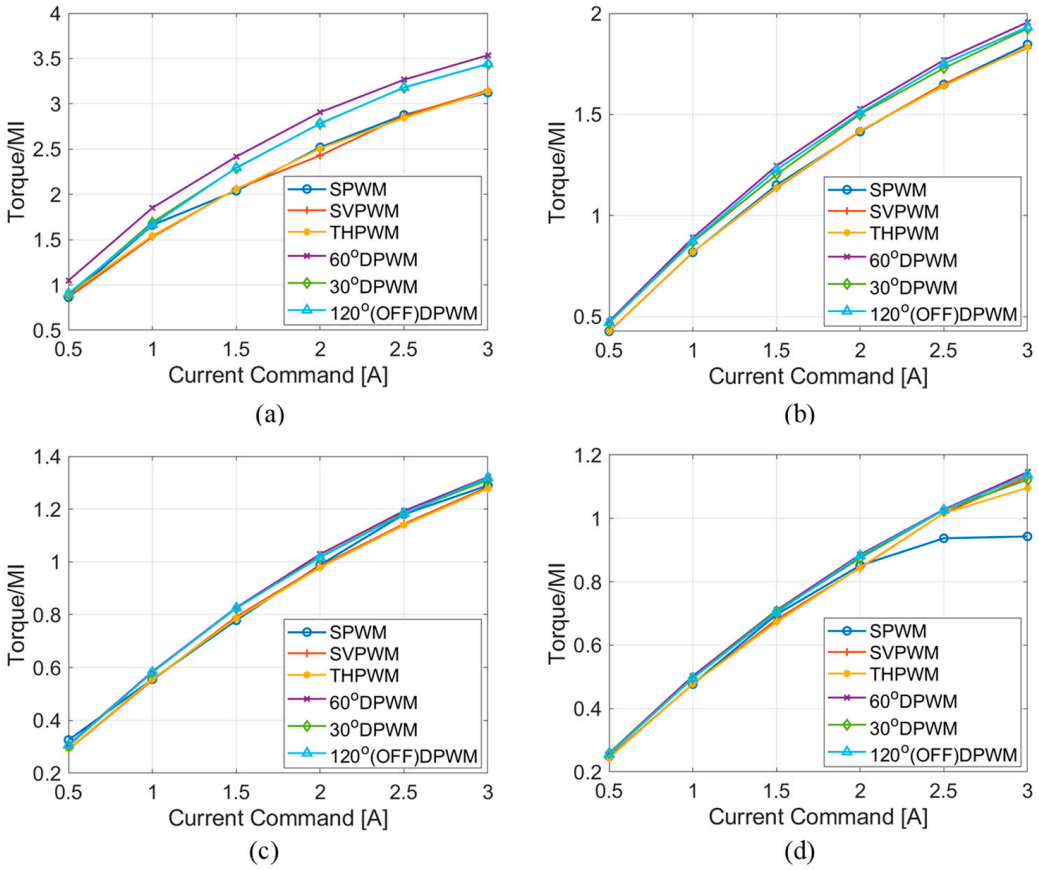

Figure 19. Experimental results of torque per MI depending on the PWM technique at (**a**) 200 rpm; (**b**) 600 rpm; (**c**) 1000 rpm; (**d**) 1200 rpm.

In Figure 20a, the inverter efficiency of the 60° DPWM is 1–3% higher than that of other methods at low speed. In addition, the efficiency of the 30° DPWM and the 120° DPWM decreases in the low-torque region, but as the torque increases, there is no significant difference in efficiency compared to other methods. On the other hand, as shown in Figure 20b, the efficiency of the 60° DPWM and the 30° DPWM at 600 rpm is about 0.5% higher than others. In Figure 20c, the efficiency of the 120° (off) DPWM and the 30° DPWM at 1000 rpm is slightly higher than others, but that of THPWM is about 1% lower than other methods. From the results in Figure 20, PWM performance varies according to speed and torque region, and selecting an appropriate method in the control domain will help to improve efficiency. In addition, it needs to analyze the characteristics above the rated region, that is, in the field-weakening area.

Unlike simulations using ideal sine wave back EMF, the actual motor back EMF includes harmonics. Therefore, the current and torque of the motor vary according to the back EMF waveform. Additionally, harmonic components appear larger in the experimental results than in the simulations. According to the test results, the trends of the current harmonics and the efficiency also vary depending on the speed and load of the motor. In the case of the 120° DPWM, the number of switches is reduced compared to other methods, but relatively high harmonics are caused. However, as shown in Figure 20, the inverter efficiency is similar to other methods. However, the noise or vibration due to the second

and fifth harmonics will be larger than other methods in high-speed driving, and therefore the 120° DPWM will be a better selection in the low-speed region than high-speed. In the case of SPWM and SVPWM, the fundamental component is high, but the harmonics are low, therefore it will be a good selection at the high-speed region. However, since the motor cannot be driven in the overmodulation region with SPWM, SVPWM should be selected for the overmodulation region control.

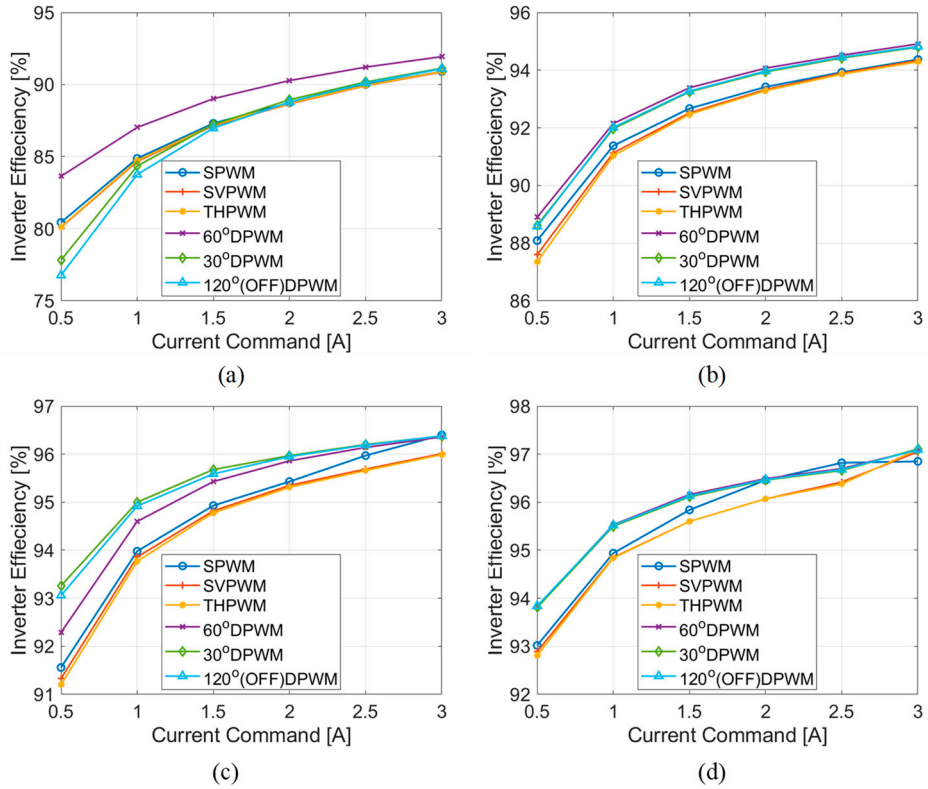

Figure 20. Experimental results of the inverter efficiency depending on the PWM technique at (**a**) 200 rpm; (**b**) 600 rpm; (**c**) 1000 rpm; (**d**) 1200 rpm.

5. Conclusions

This study analyzed the characteristics of IPMSM by the PWM techniques. The PWM techniques considered in this study are commonly used in all industries. Since some PWM techniques are complicated for construction, the offset voltage injection method is used for the experiments. The results with the offset voltage injection method are not much different from those without. Therefore, since it can be constructed with a relatively simple algorithm, it will have a good influence on selecting a PWM technique in the future.

In particular, the control performance of each PWM was confirmed through current harmonics and torque ripple analysis according to the operating range of the IPMSM. Additionally, the performance was validated by measuring the motor and inverter efficiencies depending on various PWM techniques for the IPMSM. Speed control was performed according to the speed and load of the motor, and phase current and efficiency were measured in each test. From the results, the CPWM technique had a higher MI than that of DPWM but a lower inverter efficiency. However, motor performance varied depending on the operating speed, load torque, and PWM method. It is important to select the proper PWM method according to speed and load, and it is more important in the case of operating over the rated speed.

Author Contributions: Conceptualization, H.-J.P. and H.-W.A.; methodology, H.-J.P. and H.-W.A.; software, H.-J.P. and H.-W.A.; validation, H.-J.P., H.-W.A. and S.-C.G.; formal analysis, H.-W.A.; investigation, H.-J.P.; resources, H.-J.P.; data curation, H.-J.P.; writing—original draft preparation, H.-J.P.; writing—review and editing, H.-J.P., H.-W.A. and S.-C.G.; visualization, H.-J.P. and H.-W.A.; supervision, S.-C.G.; project administration, S.-C.G.; funding acquisition, S.-C.G. All authors have read and agreed to the published version of the manuscript.

Funding: This work was supported by the National Research Foundation of Korea(NRF) grant funded by the Korea government(MSIT) (No. 2020R1C1C1011001).

Data Availability Statement: The data presented in this study are available on request from the corresponding author. The data are not publicly available due to ongoing studies.

Conflicts of Interest: The authors declare no conflict of interest.

References

1. Ferreira, F.; Baoming, G.; Almeida, A. Reliability and Operation of High-Efficiency Induction Motors. *IEEE Trans. Ind. Appl.* **2016**, *52*, 4628–4637. [CrossRef]
2. Vratislav, M. Three-Level PWM Floating H-Bridge Sinewave Power Inverter for High-Voltage and High-Efficiency Applications. *IEEE Trans. Pow. Electron.* **2016**, *31*, 4065–4074.
3. Khan, A.A.; Cha, H. Dual-Buck-Structured High-Reliability and High Efficiency Single-Stage Buck–Boost Inverters. *IEEE Trans. Ind. Electron.* **2018**, *65*, 3176–3187. [CrossRef]
4. Chun, T.W.; Ahn, J.R.; Lee, H.H.; Kim, H.G.; Nho, E.C. A Novel Strategy of Efficiency Control for a Linear Compressor System Driven by a PWM Inverter. *IEEE Trans. Ind. Electron.* **2008**, *55*, 296–301. [CrossRef]
5. Jun, H.W.; Lee, J.; Lee, H.W.; Kim, W.H. Study on the Optimal Rotor Retaining Sleeve Structure for the Reduction of Eddy-Current Loss in High-Speed SPMSM. *IEEE Trans. Magn.* **2015**, *51*, 1–4. [CrossRef]
6. Tabora, J.; Tostes, M.; Bezerra, U.; Matos, E.; Filho, C.; Soares, T.; Rodrigues, C. Assessing Energy Efficiency and Power Quality Impacts Due to High-Efficiency Motors Operating Under Nonideal Energy Supply. *IEEE Access* **2021**, *9*, 121871–121882. [CrossRef]
7. Dementyev, Y.; Bragin, A.; Kojain, N.; Udut, L. Control System with Sinusoidal PWM Three-Phase Inverter with a Frequency Scalar Control of Induction Motor. In Proceedings of the 2015 International Siberian Conference on Control and Communications, Omsk, Russia, 21–23 May 2015.
8. Hari, V.; Narayanan, G. Space-Vector-Based Hybrid PWM Technique to Reduce Peak-to-Peak Torque Ripple in Induction Motor Drives. *IEEE Trans. Ind. Appl.* **2016**, *52*, 1489–1499.
9. Reddy, N.; Reddy, T.; SubbaRayudu, D. Space Vector Based Minimum Switching Loss PWM Algorithms for Vector Controlled Induction Motor Drives. In Proceedings of the 2010 Joint International Conference on Power Electronics, Drives and Energy Systems & 2010 Power India, New Delhi, India, 20–23 December 2010.
10. Pinto, J.; Bose, B.; Silva, L.; Kazmierkowski, M. A Neural-Network-Based Space-Vector PWM Controller for Voltage-Fed Inverter Induction Motor Drive. *IEEE Trans. Ind. Appl.* **2000**, *36*, 1628–1636.
11. Hari, V.; Narayanan, G. Theoretical and Experimental Evaluation of Pulsating Torque Produced by Induction Motor Drives Controlled With Advanced Bus-Clamping Pulsewidth Modulation. *IEEE Trans. Ind. Electron.* **2016**, *63*, 1404–1413. [CrossRef]
12. Holtz, J. Pulsewidth modulation-a survey. *IEEE Trans. Ind. Electron.* **1992**, *39*, 410–420. [CrossRef]
13. Holtz, J. Pulsewidth modulation for electronic power conversion. *Proc. IEEE* **1994**, *82*, 1194–1214. [CrossRef]
14. Krah, J.-O.; Holtz, J. High-performance current regulation and efficient PWM implementation for low-inductance servo motors. *IEEE Trans. Ind. Appl.* **1999**, *35*, 1039–1049. [CrossRef]
15. Qu., L.; Qu, L.; Qiao, W.; Zhang, Z. Zero Voltage Vector Selection in a Saturation Controller-Based Direct Torque Control for Permanent-Magnet Synchronous Motors. In Proceedings of the 2019 IEEE Energy Conversion Congress and Exposition, Baltimore, MD, USA, 29 September–3 October 2019.
16. Bhavani, J.; Amarnath, J.; Rayudu, D. Generalized PWM algorithm for VSI fed Induction Motor Drives Using the only Sampled Reference Phase Voltages. In Proceedings of the 2012 IEEE 5th India International Conference on Power Electronics, Delhi, India, 6–8 December 2012.
17. Perron, M.; Le-Huy, H. Full Load Range Neural Network Efficiency Optimization of an Induction Motor with Vector Control using Discontinuous PWM. In Proceedings of the 2006 IEEE International Symposium on Industrial Electronics, Montreal, QC, Canada, 9–13 July 2006.
18. Sun, Y.; Li, S.; Fu, X.; Dong, W.; Ramezani, M.; Balasubramanian, B. Approximate Dynamic Programming Vector Controllers for Operation of IPM Motors in Linear and Overmodulation Regions. *IEEE Trans. Tran. Electron.* **2021**, *7*, 659–670. [CrossRef]
19. Mohan, P.; Reddy, T.; Kumar, M. A High-Performance PWM Algorithm for Vector Controlled Induction Motor Drive for Reduced Current Ripple. In Proceedings of the IEEE International Conference on Recent Advances and Innovations in Engineering, Jaipur, India, 9–11 May 2014.
20. Grandi, G.; Loncarski, J.; Srndovic, M. Analysis and Minimization of Output Current Ripple for Discontinuous Pulse-Width Modulation Techniques in Three-Phase Inverters. *Energies* **2016**, *9*, 380. [CrossRef]

21. Tcai, A.; Shin, H.U.; Lee, K.B. DC-Link Capacitor-Current Ripple Reduction in DPWM-Based Back-to-Back Converters. *IEEE Trans. Ind. Electron.* **2018**, *65*, 1897–1907. [CrossRef]
22. Marouani, K.; Khaldi, M.; Khoucha, F.; Kheloui, A. Switching Losses and Harmonic Currents Evaluation of PWM Tech-niques for VSI-Fed Dual Stator Induction Motor Drive. In Proceedings of the 17th Mediterranean Conference on Control & Au-Tomation, Thessaloniki, Greece, 24–26 June 2009.
23. Un, E.; Hava, A. A Near-State PWM Method With Reduced Switching Losses and Reduced Common-Mode Voltage for Three-Phase Voltage Source Inverters. *IEEE Trans. Ind. Appl.* **2009**, *45*, 782–793. [CrossRef]
24. Wu, Y.; Shafi, M.; Knight, A.; McMahon, R. Comparison of the Effects of Continuous and Discontinuous PWM Schemes on Power Losses of Voltage-Sourced Inverters for Induction Motor Drives. *IEEE Trans. Pow. Electron.* **2011**, *26*, 182–191. [CrossRef]
25. Zhang, G.; Wan, Y.; Wang, Z.; Gao, L.; Zhou, Z.; Geng, Q. Discontinuous Space Vector PWM Strategy for Three-Phase Three-Level Electric Vehicle Traction Inverter Fed Two-Phase Load. *World Electr. Veh. J.* **2020**, *11*, 27. [CrossRef]
26. Piazza, M.; Pucci, M.; Vitale, G. Benchmarking of PWM Techniques Effects on Efficiency, Power Quality and EMI in DC-supplied Induction Motor Drives. In Proceedings of the 2013 IEEE Energy Conversion Congress and Exposition, Denver, CO, USA, 15–19 September 2013.
27. Albatran, S.; Allabadi, A.; Khalaileh, A.; Fu, Y. Improving the Performance of a Two-Level Voltage Source Inverter in the Overmodulation Region Using Adaptive Optimal Third Harmonic Injection Pulsewidth Modulation Schemes. *IEEE Trans. Pow. Electron.* **2021**, *36*, 1092–1103. [CrossRef]
28. Schoonhoven, G.; Uddin, M. Harmonic Injection-Based Adaptive Control of IPMSM Motor Drive for Reduced Motor Current THD. *IEEE Trans. Ind. Appl.* **2017**, *53*, 483–491. [CrossRef]
29. Choi, J.-Y.; Park, Y.-S.; Jang, S.-M. Experimental Verification and Electromagnetic Analysis for Performance of Interior PM Motor According to Slot/Pole Number Combination. *IEEE Trans. Magn.* **2012**, *48*, 987–990. [CrossRef]
30. Hava, A.M.; Kerkman, R.J.; Lopo, T.A. A High-Performance Generalized Discontinuous PWM Algorithm. *IEEE Trans. Ind. Appl.* **1998**, *34*, 1059–1071. [CrossRef]